The Adequacy of Observing Systems in Monitoring the Atlantic Meridional Overturning Circulation and North Atlantic Climate

S. ZHANG, A. ROSATI, AND T. DELWORTH

Geophysical Fluid Dynamics Laboratory, Princeton University, Princeton, New Jersey

(Manuscript received 16 February 2010, in final form 14 May 2010)

ABSTRACT

The Atlantic meridional overturning circulation (AMOC) has an important influence on climate, and yet adequate observations of this circulation are lacking. Here, the authors assess the adequacy of past and current widely deployed routine observing systems for monitoring the AMOC and associated North Atlantic climate. To do so, this study draws on two independent simulations of the twentieth century using an Intergovernmental Panel on Climate Change (IPCC) Fourth Assessment Report (AR4) coupled climate model. One simulation is treated as "truth" and is sampled according to the observing system being evaluated. The authors then assimilate these synthetic "observations" into the second simulation within a fully coupled system that instantaneously exchanges information among all coupled components and produces a nearly balanced and coherent estimate for global climate states including the North Atlantic climate system. The degree to which the assimilation recovers the truth is an assessment of the adequacy of the observing system being evaluated. As the coupled system responds to the constraint of the atmosphere or ocean, the assessment of the recovery for climate quantities such as Labrador Sea Water (LSW) and the North Atlantic Oscillation increases the understanding of the factors that determine AMOC variability. For example, the low-frequency sea surface forcings provided by the atmospheric and sea surface temperature observations are found to excite a LSW variation that governs the long-time-scale variability of the AMOC. When the most complete modern observing system, consisting of atmospheric winds and temperature, is used along with Argo ocean temperature and salinity down to 2000 m, a skill estimate of AMOC reconstruction is 90% (out of 100% maximum). Similarly encouraging results hold for other quantities, such as the LSW. The past XBT observing system, in which deep-ocean temperature and salinity were not available, has a lesser ability to recover the truth AMOC (the skill is reduced to 52%). While these results raise concerns about the ability to properly characterize past variations of the AMOC, they also hold promise for future monitoring of the AMOC and for initializing prediction models.

1. Introduction

Model studies indicate that the Atlantic meridional overturning circulation (AMOC) plays an important role in decadal climate fluctuations in the Northern Hemisphere (Zhang et al. 2006), including Atlantic hurricane activity (Goldenberg et al. 2001) and flood and drought in North America (Enfield et al. 2001), Europe (Sutton and Hodson 2005), and northern Africa (Folland et al. 1986). Recent advances in observations (Kanzow et al. 2007; Bryden et al. 2005) and simulations (Delworth et al. 1993; Delworth 1996; Jungclaus et al. 2005; Eden and Jung 2001; Griffies and Bryan 1997; Delworth and Mann 2000;

Delworth and Greatbatch 2000; Johnson et al. 2007) in coupled general circulation models (CGCMs) have enhanced our understanding of the AMOC. As a central component of the North Atlantic climate system, the AMOC is closely associated with climatological features and low frequency variability of the atmosphere and ocean in the Atlantic domain (Fig. 1)—notably the atmospheric North Atlantic Oscillation (NAO), Labrador Sea Water (LSW), Greenland–Iceland–Norwegian (GIN) seawater (GSW), and the North Atlantic subpolar–subtropical gyre system (NAG). The NAO provides a strong driving forcing for LSW and GSW, which in turn affects formation of North Atlantic Deep Water (NADW) and the AMOC. The NAG directly influences poleward heat and salt transport, NADW formation (Hilmer and Jung 2000), and the meridional overturning (Hátún et al. 2005). However, neither observations nor modeling has provided a

Corresponding author address: Shaoqing Zhang, GFDL/NOAA, Princeton University, P.O. Box 308, Princeton, NJ 08542.
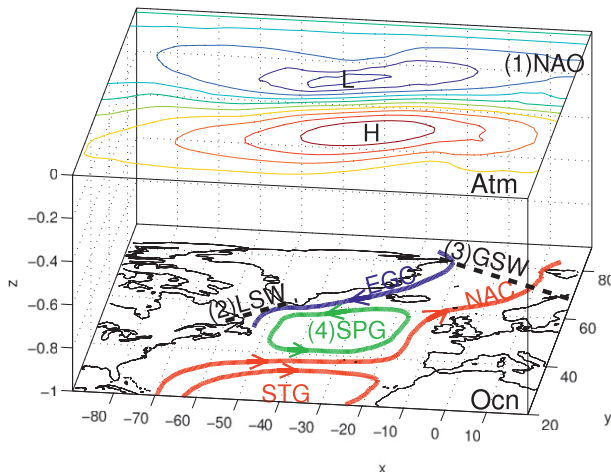E-mail: shaoqing.zhang@noaa.gov

FIG. 1. Schematic of the North Atlantic climate system, characterized by the Atlantic meridional overturnig circulation (AMOC), which is a coupled product by the atmospheric North Atlantic Oscillation, oceanic deep convection in the Labrador Sea and Greenland–Iceland–Norweigian seas as well as the North Atlantic subpolar–subtropical gyre system (NAG). Given a certain atmospheric and/or oceanic observing system, the coupled data assimilation system is expected to resolve these circulations to some extent through instantaneously exchanging information among all coupled components. The top (bottom) of the box represents the atmospheric (oceanic) circulation systems over the North Atlantic (NA) domain. The typical NAO pattern [marked by (1)] shown in the top is the first mode of EOF of the 30-yr monthly NA surface pressure anomalies of the model simulation serving as the truth. The thick dashed black lines marked by (2) and (3) indicate the position of a vertical section where LSW and GSW are identified between two isopycnal surfaces. The cyclonic subpolar gyre (green) and anticyclonic subtropical gyre (red) system in the North Atlantic Ocean are represented by (4). NAC and EGC stand for the Norwegian Atlantic Current and the East Greenland Current, respectively.

complete picture of the AMOC in time and space, and our knowledge of the basic features of AMOC and its mechanism in the real world still remains limited. In particular, how has the AMOC varied in the past and how can its future evolution be predicted?

Understanding of historical AMOC variations and initialization of coupled climate models is critical for the prediction of the AMOC. Various approaches have been used to reconstruct the AMOC history by combining instrumental data with model dynamics. Wunsch and Heimbach (2006) estimated variability of the AMOC by correcting surface forcings to obtain ocean states close to observed data based on an adjoint method defined on a long time window. Balmaseda et al. (2007b) reconstructed the ocean states directly using observed ocean data with a sequential approach in terms of optimal interpolation. Both have shown some promising results. However, it remains unclear how adequate the existing observing system is to represent and monitor the North Atlantic

climate system and whether the estimated ocean states are optimal for initializing CGCMs for numerical climate prediction. Also, the infrequency of direct measurements of the AMOC and the presence of model bias make it difficult to evaluate the reconstructed AMOC and related North Atlantic climate system quantitatively. Here we apply an ensemble-coupled data assimilation (ECDA) system (Zhang et al. 2007) to perfect model experiments for studying the adequacy of the temporally varying climate observing system in monitoring the AMOC and North Atlantic climate. Based on a certain observing system, through sufficiently blending data into coupled model dynamics, the fully coupled ensemble assimilation here pursues a balanced and coherent climate estimation in a probabilistic approach in which the ensemble mean serves as the best estimate, and all higher-order moments measure the uncertainty of the estimate.

After the description of the model and assimilation method used in section 2, section 3 presents a particular observation system simulation experiment based on existing observing networks. The numerical results about the accuracy of existing observing systems to monitor the AMOC and North Atlantic climate system are presented and discussed in section 4. Summary and discussions are given in section 5.

2. Model and assimilation method

a. A fully coupled GCM

The coupled model used in this study is a B-grid (Wyman 1996) finite difference atmospheric model [the second-generation Geophysical Fluid Dynamics Laboratory (GFDL) global atmosphere and land model (AM2–LM2), GFDL Global Atmospheric Model Development Team (2004)] coupled with the fourth version of the Modular Ocean Model (MOM4) (Griffies et al. 2005). This is one of two GFDL Intergovernmental Panel on Climate Change Fourth Assessment Report (AR4) models, called the Climate Model version 2.0 (CM2.0) (Randall et al. 2007, chapter 8). The atmosphere model has 24 vertical levels and 2.5° longitude by 2° latitude horizontal resolution. The physics package includes a K-profile planetary boundary layer (Lock et al. 2000), relaxed Arakawa–Schubert convection (Moorthi and Suarez 1992), and a simple local parameterization of the vertical momentum transport by cumulus convection. The ocean model is configured with 50 vertical levels, 22 levels having uniform 10-m thickness in the top 220 m, and 1° × 1° horizontal resolution telescoping to $1/3°$ meridional spacing near the equator. The model has an explicit free surface with a freshwater flux exchange between the atmosphere and ocean. Parameterized physical processes include k-profile parameterization vertical mixing, neutral
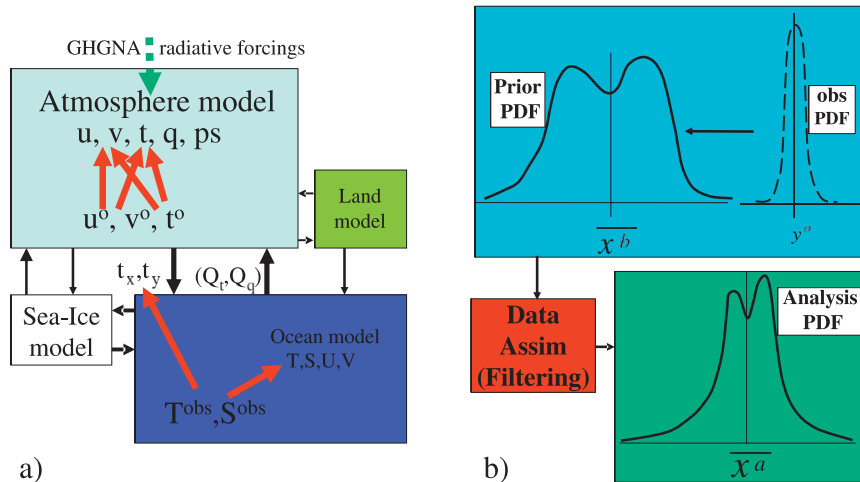
FIG. 2. Cartoon of how (a) data assimilation (red arrows) in the GFDL coupled model transfers observational information into the coupled atmosphere–ocean–land–sea ice component by exchange fluxes (black arrows), and (b) an ensemble filter updates the probability distribution for a scalar variable. The green arrow in (a) denotes the radiative forcings expressed by the atmospheric greenhouse gas and natural aerosol (GHGNA), and the dashed line means that the GHGNA radiative forcings in the assimilation may be set as a fixed year (1860). The red arrows in (a) indicate that the oceanic observations are allowed to impact all oceanic-state variables including the wind stresses at the sea surface, and the reanalysis atmospheric temperature and wind are allowed to make a cross adjustment among the temperature and wind. (top) Here, (b) represents (left) the prior distribution derived from model ensemble integrations starting from the previous assimilation results and (right) an observational distribution (usually Gaussian). (bottom) In (b), (left) an ensemble-filtering process combines the observational and prior distributions to form (right) an updated so-called analyzed distribution realized by the states of a set of ensemble members, which are initial conditions for the next ensemble integrations.

physics, a spatially dependent anisotropic viscosity, and a shortwave radiative penetration depth that depends on a prescribed climatological ocean color. Insolation varies diurnally and the wind stress at the ocean surface is computed using the velocity of the wind relative to the surface currents. An efficient time-stepping scheme (Griffies 2005) is employed. More details can be found in Gnanadesikan et al. (2006) and Griffies et al. (2005). The Sea Ice Simulator in the coupled model is a dynamical ice model with three vertical layers (one for snow and two for ice) and five ice thickness categories. The elastic–viscous–plastic technique (Hunke and Dukowicz 1997) is used to calculate ice internal stress, and the thermodynamics is a modified Semtner three-layer scheme (Winton 2000). The coupled components of this model interact with each other through exchanged fluxes (Fig. 2a).

b. An ECDA system

Ensemble coupled data assimilation (ECDA) estimates the probability distribution function (PDF) of climate states by combining the prior PDF derived from coupled model dynamics and the observational PDF (schematically illustrated in Fig. 2b) (Jazwinski 1970).

The prior PDF is discretely represented by a set of ensemble model integrations that run in parallel. Filtering is implemented by a multivariate linear regression that projects an observational increment onto all correlated model variables using the temporally varying error covariance computed from the model ensemble (Anderson 2003; Zhang and Anderson 2003). This multivariate data projection maintains mostly physical balances such as the geostrophy in the atmosphere and the T–S relationship in the ocean (Kalnay 2003). The data projection only adjusts the prior PDF up to the second-order moment, and all higher-order moments remain (Anderson 2003). Thus, the filtering is expected to maintain the nonlinearity of climate evolution such as the bimodal character in the regime transition of AMOC. Also, the ECDA framework allows all coupled components to be adjusted by data through instantaneously exchanging information among them (see the illustration in Fig. 2a). It is expected to produce an optimal estimate of the coupled model ensemble by sufficiently blending data into model dynamics (Zhang et al. 2007). In this way, the ensemble mean is the estimate for the state, and all higher-order moments measure the uncertainty of the estimate. The ensemble

TABLE 1. Five typical climate observing systems from the twentieth century to the twenty-first century. Note the following: early (E); middle (M); later (L); and for simplicity only 30°S–30°N SST is used here without destroying the high latitude's water property by excluding direct SST insertion there (SST_t).

Obs system	Atmosphere		Ocean		Historical period	Data constraints
	Data*	Format	Data	Format		
O_{SSTt}^{Atm}	u, v, T	Reanalysis gridded	SST_t	Gridded	Twentieth–twenty-first century	Surface forcings driving deep oceans
O_{XBT}	—	—	SST_t, XBT, CTD MBT, OSD MRB	Gridded or in situ	ML Twentieth century	Twentieth century ocean-only observing system
O_{XBT}^{Atm}	u, v, T	Reanalysis gridded	SST_t, XBT, CTD MBT, and OSD MRB	Gridded or in situ	ML Twentieth century	Twentieth century climate observing system
O_{Argo}	—	—	SST_t Argo	Gridded or in situ	Twenty-first century	Twenty-first century ocean-only observing system
O_{Argo}^{Atm}	u, v, T	Reanalysis gridded	SST_t Argo	Gridded or in situ	Twenty-first century	Twenty-first century climate observing system

* Atmospheric data include only reanalysized temperature and wind to simulate the present atmospheric observing system that lacks sufficient and reliable moisture observations, reflecting the fact that cloud in the atmosphere modeling is the largest uncertainty.

data assimilation is tested using 6, 12, and 24 members, and no significant improvement is found from 12 to 24 members. Based on the test results, all ECDA experiments are performed with a 12-member ensemble that is used to compute the state estimation (ensemble mean) and spread of the estimate. It is worth mentioning that test results show that the reconstruction has a small sensitivity on the initial states at the differing point of the control (CTL), from which the assimilation starts, as well as external radiative forcings used in the assimilation model.

3. Simulation of temporally evolving ocean observing system

a. Temporal evolution of ocean observations

The ocean observing system has been built up over time, but historically the subsurface ocean has been observed very sparsely. The recent deployment of a global array of profiling floats by the Argo (Array for Real-Time Geostrophic Oceanography) program (available online at http://www.argo.ucsd.edu) provides potentially an advance in our ability to monitor ocean heat content (see e.g., Ivchenko et al. 2006) and density variability. It is important to understand how this nonstationary system impacts the detection of decadal variability. For example, the temporally evolving nature of the ocean observing system, particularly due to the paucity of salinity data in XBT as well as XBT data only going to 500-m depth, may give rise to spurious decadal variability, making difficulties in the assessment of the monitoring. One simplified way to study this issue is by observing system simulation

experiments within a perfect model framework for each period. In particular, we want to contrast the twentieth-century XBT network with the twenty-first-century Argo network. The twentieth-century XBT profiles are largely the same as used by Levitus et al. (2005) for the World Ocean Analysis (WOA), mainly from XBT, but also including CTD, drifting buoy (DRB), Ocean Weather Station data (OSD), undulating oceanographic recorder (UOR), and moored buoy (MRB), hereafter briefly called XBT. Throughout this paper we will use the notation O with a subscript (superscript) representing the oceanic (atmospheric) observing network, so O_{XBT}^{Atm} is the XBT network with atmospheric variables and O_{Argo}^{Atm} is the Argo network with atmospheric variables. Beside O_{XBT}^{Atm} and O_{Argo}^{Atm} three additional observing systems (see Table 1) are also used to simulate the evolution of climate observations from preindustrial to present: O_{SSTt}^{Atm}—atmospheric winds and temperature plus tropical sea surface temperature (SSTt); O_{XBT}—the twentieth-century ocean alone temperature observations; and O_{Argo}—the twenty-first-century temperature and salinity network (Argo). While the O_{SSTt}^{Atm} system provides only the sea surface forcings for the ocean, which consists of constraints of the atmospheric wind and temperature and tropical SSTs, the other four observing systems directly constrain the subsurface ocean to some extent. The older twentieth-century O_{XBT} system has data primarily along commercial shipping routes (Fig. 3a), with ocean temperatures sampled only down to a depth of 500 m (except for a small amount of CTDs and OSDs that go deeper; Fig. 3d). The more recent twenty-first-century O_{Argo} system deploys a more regular network (Figs. 3b,c) that samples both temperature and salinity down to 2000 m
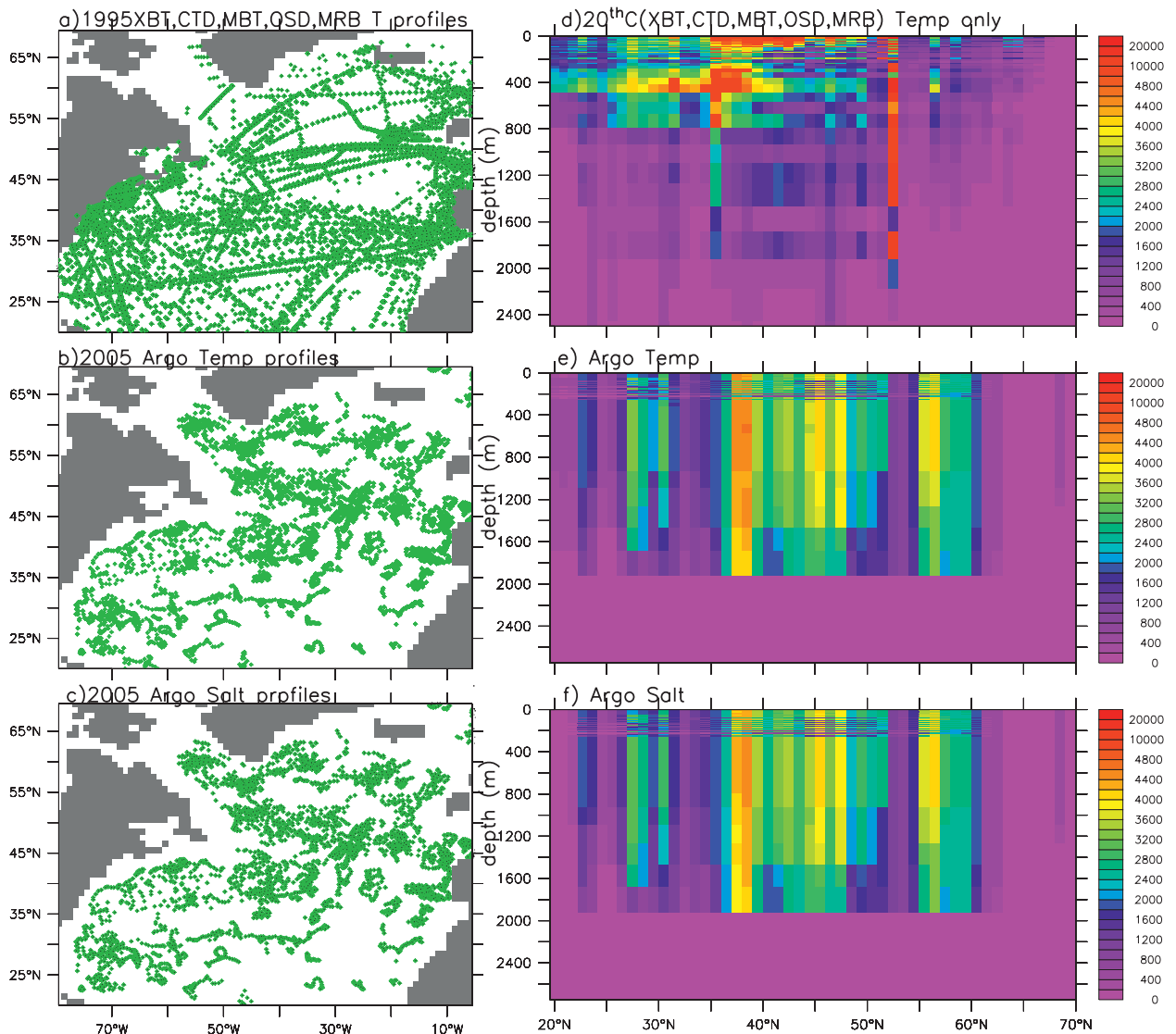
FIG. 3. The coverage of observed profiles of (a) 1995 including XBT, CTD, MBT, OSD, and MRB; (b) 2005 Argo temperature; and (c) 2005 Argo salinity in the North Atlantic domain and distribution of observed profile numbers in the North Atlantic channel for (d) XBT, CTD, MBT, OSD, and MRB; (e) Argo temperature; and (f) Argo salinity. Each number in a y–z model gridbox represents the sum of profiles in all grid boxes with the same latitude and depth bounds over the period of 1976–2000. The 2005 Argo network is repeatedly used to simulate a temporally evolving Argo network. Note the discontinuities in both XBT and Argo reflect the synthetic effect of the difference of model and observation resolutions, as well as the observation quality control. Also note that while this figure shows an example of the distribution of subsampling locations in the North Atlantic domain, global observational data are used in all assimilation experiments in this study.

(Figs. 3e,f), in which a roughly global coverage began with 2003 and the full deployment finished in 2007. It is worth noting that MRB, an important array to monitor the tropical ocean in the twentieth-century ocean observing network, began in the early 1980s.

b. Experimental design in perfect model framework

Model bias has been recognized as a serious obstacle to reliable representation of climate variability by combining models and data (Dee and Sliva 1998; Dee 2005;

Balmaseda et al. 2007a). As a first step, we use a perfect model twin-experiment framework to avoid the complexity associated with model bias. We employ a state-of-the-art global climate model (GFDL CM2.0) and make use of multiple simulations of the twentieth century with that model. These simulations start from differing points in a long control integration and are forced with the same sets of radiative forcing changes over the twentieth and early twenty-first centuries, including changes in greenhouse gases and aerosols. The model reproduces many

aspects of the observed climate system (see Delworth et al. 2006; Gnanadesikan et al. 2006). One simulation with that model is taken as "truth." Synthetic observations (Sobs) are then created by sampling from the truth simulation using locations and times when observations were available in various observing systems. These Sobs are then assimilated into the second simulation. The degree to which the assimilation of Sobs is able to constrain the second simulation, such that it reproduces the truth simulation, is then taken as a measure of the adequacy of the observing system through the use of error statistics such as correlation and rms error (RMSE). We take the atmospheric reanalysis as the atmospheric observations, making the most use of great efforts having been done for the atmosphere data assimilation in the community (e.g., Kalnay et al. 1996). To simulate the availability of MRBs and the second version of the National Centers for Environmental Prediction (NCEP)–National Center for Atmospheric Research (NCAR) atmospheric reanalysis and to leave a few years as a spinup time for ocean data assimilation, we set the 1976–2005 truth simulation as the target that the assimilations using various observing systems try to recover.

In this perfect model study, the standard IPCC historical simulation that starts from a 300-yr spinup integration initialized from the previous integration (h_1) (Stouffer et al. 2004) is set as truth, whereas another historical simulation that starts from a 380-yr spinup integration initialized from the previous integration (h_3) is set as the Control. Specifically, the daily ocean temperature or temperature and salinity are extracted from the truth simulation over the period 1976–2005 so that the truth is sampled by a particular observing system according to times and locations where observations were available. The sampling process is basically a trilinear interpolation, added by white noise to simulate random observational errors (Zhang et al. 2007; 2009). The standard deviation of the white noise is 0.5°C for temperature and 0.1 psu for salinity at the sea surface and exponentially decays to zero by 2000 m. The atmospheric Sobs are the "reanalysis" daily model-gridded atmospheric temperature and wind fields with added white noise, which have a standard deviation of 1°C for temperature and 1 m s^{-1} for velocities. Starting from 1 January 1976 we assimilate the Sobs into the second CM2.0 simulation of the twentieth century (we call this second simulation the Control), and evaluate the degree to which the observations constrain the second simulation to reproduce the truth simulation by conducting error statistics referred to as the truth. Note that, while the temporally evolving twentieth-century XBT observing network (1976–2005) is used in this study, the Argo network in 2005, which has moderate coverage of the Argo deployment, is repeatedly used to simulate the

evolution of the twenty-first-century Argo observing system. It is worth mentioning that use of the 2005 network may underestimate the monitoring skill of the Argo system compared to the case with the full deployment, which is unavailable for the assimilation over a few decades required for error statistics to evaluate the monitoring adequacy. However, given the scope of this study, it will not change the conclusions we drawn from the these experiments.

4. Adequacy of monitoring the AMOC and North Atlantic climate in various observing systems

Applying each observing system into ECDA, we assess how well a given observing system can recover the variability and strength of the AMOC and related aspects of the North Atlantic climate system (Fig. 1). We define the AMOC index as the maximum value of the overturning streamfunction between 40°–70°N in the North Atlantic section. The LSW (GSW) index is defined as the averaged thickness between two isopycnal surfaces $\sigma_{1.5} = 34.62$ and 34.56 (34.96 and 34.86) in the vertical section denoted by (2) LSW [(3) GSW] in Fig. 1, which corresponds to the model-simulated deep mode water in the Labrador Sea (Fram Strait). This mode water index is also referred to as an index of deep convection in the Labrador (Greenland–Iceland–Norwegian) Sea. Note that owing to the model bias of the rather intermittent and shallow convection in the North Atlantic Ocean (Gnanadesikan et al. 2006), the model mode water is lighter than the observed annual mean (a density range for the observed annual-mean LSW is 34.62–34.72, for instance). The NAO (NAG) index is defined as the linear regression coefficient of the North Atlantic (20°–65°N) 30-yr surface pressure anomaly (SPA) [sea surface height anomaly (SSHA)] onto the first mode of the empirical orthogonal function of SPA (Thompson and Wallace 2000) (SSHA) (Häkkinen and Rhines 2004) of the truth simulation.

The time series of the defined NAO, NAG, LSW, GSW, and AMOC indices produced by two model simulations (the truth and the Control) and the estimates from five observing systems (O_{SSTt}^{Atm}, O_{XBT}, O_{Argo}, O_{XBT}^{Atm} and O_{Argo}^{Atm}; see Table 1) are shown in Figs. 4 and 5. The anomaly correlation coefficient (ACC) and RMSE of the circulation estimate (ensemble mean) generated from the control simulation and the assimilations based on these observing systems are listed in Table 2. In particular, to analyze the meridional transport in different data constraint schemes the vertical structure of the time-mean errors of the estimated AMOC streamfunction from the Control simulation and the five assimilations is shown in Fig. 6. Finally, we define a score of monitoring skill to measure the adequacy of each observing system to monitor each aspect of
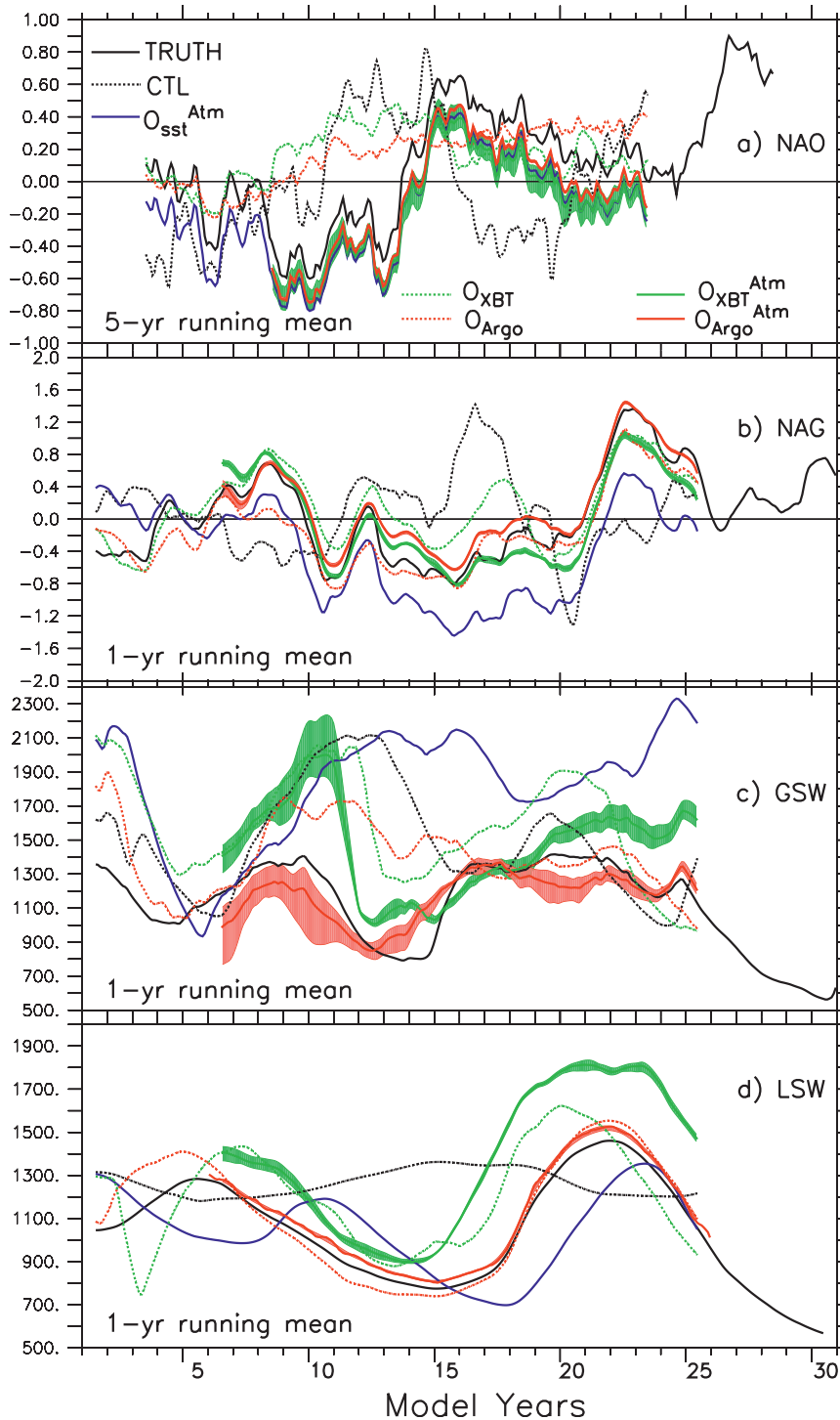
FIG. 4. Time series of (a) the atmospheric NAO, (b) NAG, (c) GSW, and (d) LSW estimated by five typical climate observing systems to simulate the evolution of the climate observing system from preindustrial to present: O_{SSTt}^{Atm} (blue), O_{XBT} (dashed green), O_{Argo} (dashed red), O_{XBT}^{Atm} (green), and O_{Argo}^{Atm} (red). The light-green and light-red shaded areas represent the corresponding ensemble spread measured by the ensemble standard deviation (see section 2b) of the assimilations using O_{XBT}^{Atm} and O_{Argo}^{Atm}. Except for the NAO index shown as a 5-yr running mean, all others are shown as 1-yr running means.
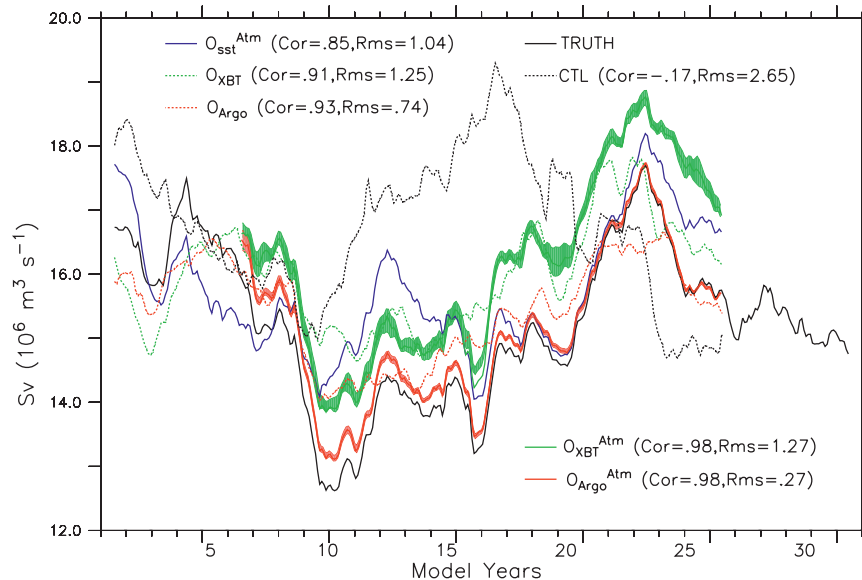
FIG. 5. Time series of the monitored AMOC by five typical climate observing systems from preindustrial to present. The observing systems (see Table 1) being evaluated are O_{SSTt}^{Atm} O_{XBT}, O_{Argo}, O_{XBT}^{Atm} and O_{Argo}^{Atm} The light-green and light-red shaded areas represent the corresponding ensemble spread measured by the ensemble standard deviation (see section 2b) of the assimilations using O_{XBT}^{Atm} and O_{Argo}^{Atm}. All statistics are based on monthly-mean data with a 1-yr running mean.

the North Atlantic climate system quantitatively. The score is defined as the normalized RMSE of an estimate by the RMSE of the Control as $[1 - \min(1, RMSE_{Assim}/RMSE_{Control})] \times 100\%$, so a 100% score attributes an observing system a perfect monitoring skill for a particular aspect of the North Atlantic climate system whereas a 0% score represents that the observing system has no monitoring skill at all for this aspect. The scores of all observing systems in monitoring the NAO, NAG, GSW, LSW, and AMOC are summarized in Fig. 7. The standard deviation (sdv) of each score evaluated from individual ensemble members, as shown in parentheses, is a measure of the uncertainty of the estimated monitoring skill.

a. NAO, NAG, LSW, and GSW

Generally, only the constraint of atmospheric observations can produce a correct phase of the NAO variations

(Fig. 4a), corresponding to a nearly perfect ACC (column 3 of Table 2). Otherwise, the NAO signal constrained by an oceanic observing system (O_{XBT} or O_{Argo}) is very weak, and the corresponding ACC is very low. While the constraint of an ocean observing system produces a good estimate for the NAG strength and phase (a small RMSE and high ACC, see columns 4 and 5), only the surface forcings (O_{SSTt}^{Atm}) cannot drive out a correct strength for the NAG (the RMSE is large) in the 30-yr assimilation period, although a roughly correct variation phase (a high ACC) is obtained for this wind-driven oceanic circulation (Fig. 4b). On the other hand, only the direct oceanic constraint from an ocean observing system can produce a high ACC for LSW, while obtaining a high ACC for GSW (>0.6, for instance) requires the constraints of both the atmosphere and ocean. Also, only the Argo observing system (O_{Argo}), which provides both temperature and salinity observations

TABLE 2. The anomaly correlation coefficient (ACC) and rms error (RMSE) produced by the assimilation of various climate observing systems for the NAO, NAG, GSW, LSW, and AMOC. The case of a free model Control without any data constraint is also listed as a reference.

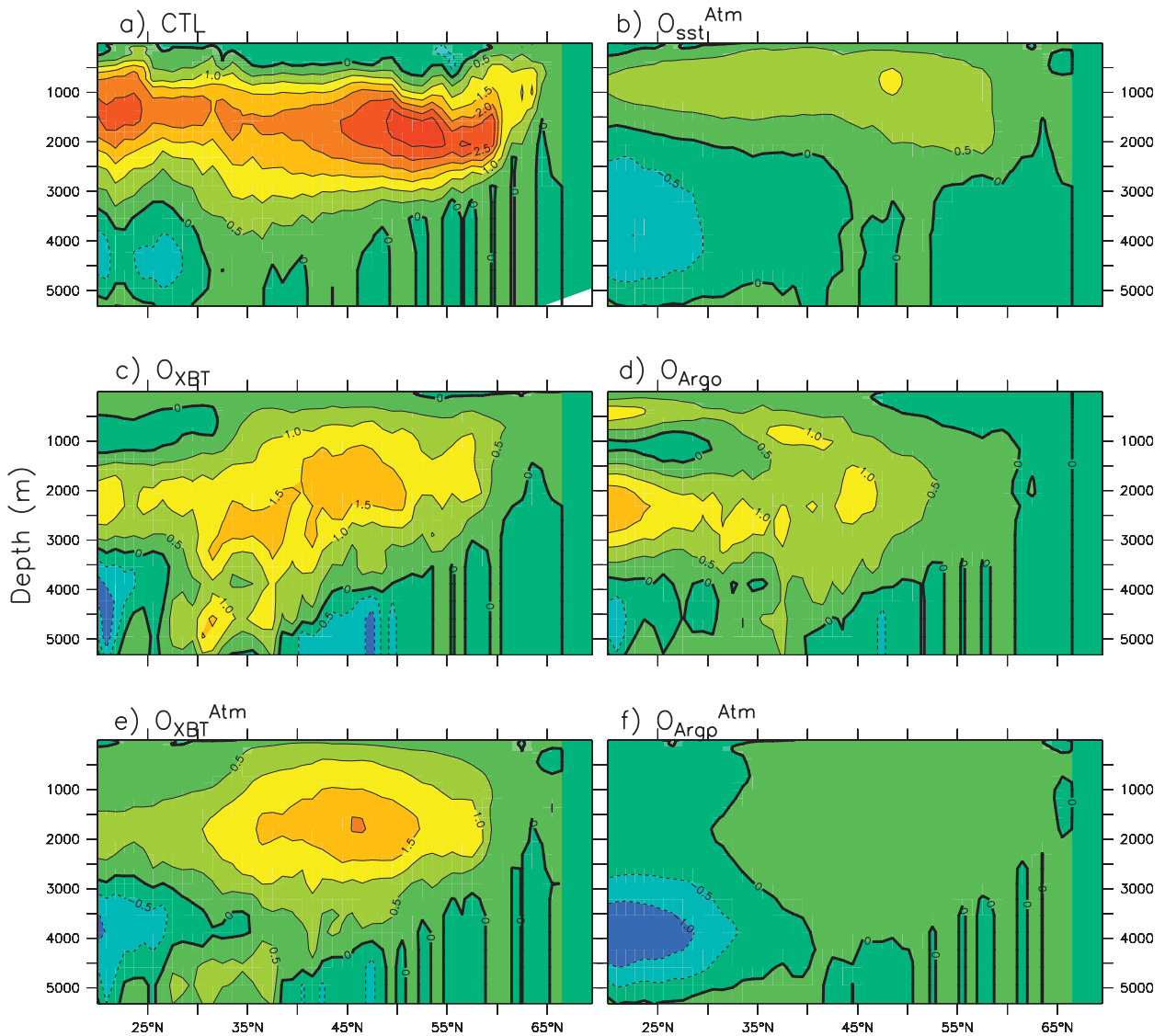| Obs system	NAO		NAG		GSW		LSW		AMOC	
	RMSE	ACC	RMSE	ACC	RMSE	ACC	RMSE	ACC	RMSE	ACC
Control	0.39	0.2	0.93	−0.3	544	−0.36	338	−0.7	2.65	−0.17
O_{SSTt}^{Atm}	0.08	1	0.63	0.95	769	0	207	0.57	1.03	0.85
O_{XBT}	0.34	0.03	0.38	0.86	461	0.41	205	0.81	1.25	0.91
O_{Argo}	0.29	0.34	0.26	0.96	352	0	55	1	0.75	0.93
O_{XBT}^{Atm}	0.08	1	0.42	0.96	315	0.68	335	0.91	1.28	0.98
O_{Argo}^{Atm}	0.06	1	0.16	1	119	0.83	44	1	0.27	0.98

FIG. 6. Vertical distribution of the time-mean errors of the AMOC streamfunction for (a) the Control (CTL) and assimilations of (b) $O_{\text{SSTt}}^{\text{Atm}}$ (c) O_{XBT}, (d) O_{Argo}, (e) $O_{\text{XBT}}^{\text{Atm}}$ and (f) $O_{\text{Argo}}^{\text{Atm}}$. Contour interval is 0.5 Sv (Sv $\equiv 10^6$ m^3 s^{-1}).

for the ocean, can significantly constrain the strength of LSW. However, without the atmospheric constraint, even the use of O_{Argo} cannot significantly recover the strength of GSW (see columns 6–9 of Table 2 and Figs. 4c,d). Next, we will analyze the response of the atmosphere and ocean to the data constraint(s) in a coupled system and try to get more understanding on these phenomena.

In the North Atlantic climate system, if we assume coupling feedbacks are not crucial (Delworth and Greatbatch 2000), the assimilation using $O_{\text{SSTt}}^{\text{Atm}}$ is largely equivalent to an ocean-only model simulation driven by surface fluxes (mostly defined by the surface air temperature and wind in this case) initialized from an ocean state in the control. This experiment helps us understand how the North Atlantic deep ocean responds to the signals in surface

forcings. Comparing the blue line to the black line in Figs. 4a and 4d, respectively, it is seen that while the assimilation of the atmosphere and tropical SST observations ($O_{\text{SSTt}}^{\text{Atm}}$) recovers the atmospheric NAO with a high accuracy and a small uncertainty (Fig. 4a and column 1 of Fig. 7), the established low-frequency NAO signals drive out a lagged LSW variation (Fig. 4d) as a free response of the ocean to the surface forcings. (Note in the targeted period of the assimilation the LSW's variations of the control happen to be out of the phase of the truth and show an ACC of −0.7.) This result shows an example that the NADW is not only the result of a barotropic adjustment of the ocean to wind forcings, and it could be associated with large-scale transport processes and sea ice activities driven by the low-frequency atmospheric forcings. However, the lagged
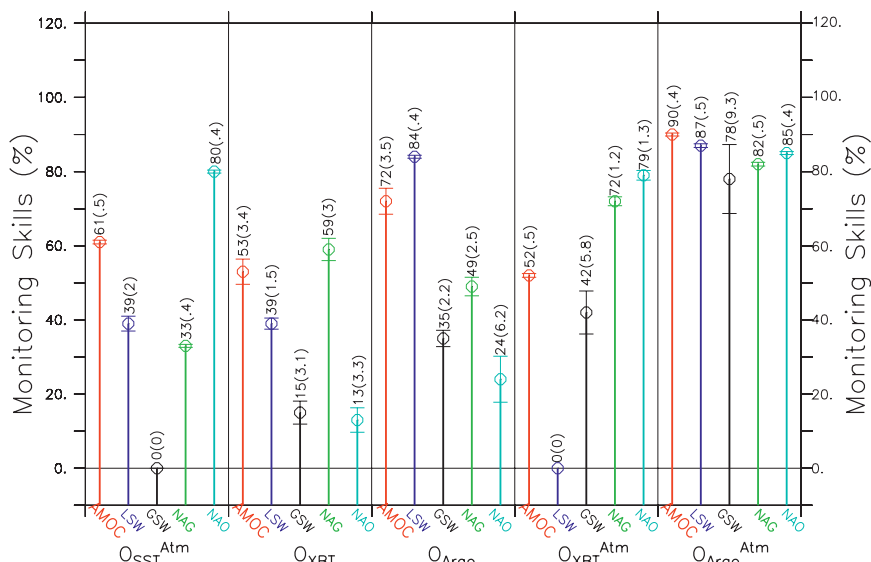
FIG. 7. Monitoring skills of AMOC, LSW, GSW, NAG, and the atmospheric NAO for the five typical climate observing systems from preindustrial to present. In the parentheses is the corresponding error bar evaluated by the 12-member ensemble (see section 2b). All statistics are based on monthly-mean data with a 1-yr running mean.

phase of LSW derived from $O_{\mathrm{SSTt}}^{\mathrm{Atm}}$ produces a large RMSE for LSW and therefore renders a very low monitoring skill (39%) as there is no subsurface observational constraint.

The assimilations using only ocean observations (O_{XBT} and O_{Argo}) solve an inverse problem of ocean modeling in a coupled system in which the ocean states are directly adjusted by projecting data-sampled signals onto the model space, and the sea surface maintains a balance with the feedbacks of the atmosphere to the adjusted ocean states. Compared to the case of only surface forcings ($O_{\mathrm{SSTt}}^{\mathrm{Atm}}$), the direct subsurface constraints in O_{XBT} and O_{Argo} significantly change the phase of LSW. While the assimilation of temperature and salinity in O_{Argo} improves the phase of LSW dramatically, the assimilation of temperature only in O_{XBT} produces a phase error of LSW almost equally large as in the assimilation of $O_{\mathrm{SSTt}}^{\mathrm{Atm}}$ but with the opposite sign. This leads to a systematic error in the mean-state strength of the Labrador Sea deep convection derived from O_{XBT}, rendering a much lower LSW monitoring skill (39%) with a bigger uncertainty (1.5% sdv) than using O_{Argo} (84% with 0.4% sdv; see columns 2 and 3 of Fig. 7). In the assimilation of O_{XBT}, salinity is adjusted using the temperature observations applied to the model background T–S relationship to construct a thermohaline structure. From the large LSW error produced by O_{XBT}, we may have a reasoning that the salinity adjustment based on a model T–S relationship is perhaps insufficient, and the Argo's direct salinity observation is therefore particularly important for reconstructing the North Atlantic climate system. This point will be

expanded more in section 4b when we analyze the accuracy of the mean state of the estimated AMOC streamfunction.

Through adding the atmospheric data constraint, the assimilations of $O_{\mathrm{XBT}}^{\mathrm{Atm}}$ and $O_{\mathrm{Argo}}^{\mathrm{Atm}}$ produce very high NAO monitoring skills with small uncertainties—that is, 80% with 1.3% sdv and 85% with 0.4% sdv, respectively (see columns 4 and 5 of Fig. 7). The monitoring skill for the NAO in $O_{\mathrm{Argo}}^{\mathrm{Atm}}$ is slightly higher than in $O_{\mathrm{XBT}}^{\mathrm{Atm}}$ which may reflect a positive impact of improved ocean conditions resolved from the Argo observations on atmospheric circulations even in the presence of a strong atmospheric data constraint. However, combining with the deficit of the oceanic temperature-only constraint, the improved surface forcings in the assimilation of $O_{\mathrm{XBT}}^{\mathrm{Atm}}$ overestimate the strong deep convection between year 18 and 25, leading to the loss of the LSW monitoring skill of $O_{\mathrm{XBT}}^{\mathrm{Atm}}$. In contrast, combined with the well-resolved North Atlantic thermohaline structure by O_{Argo}, the $O_{\mathrm{Argo}}^{\mathrm{Atm}}$ atmospheric constraint further enhances the LSW's monitoring skill up to 87%.

Compared to LSW, GSW variability has more influence from the atmospheric data constraint. On the one hand, this is probably associated with the complex mechanism of GIN Sea Mode Water formation as will be discussed more in the next section. On the other hand, the fact that the Nordic seas are the most poorly ocean-sampled areas makes it difficult to clearly understand the contribution of an oceanic constraint to GSW variability. This area has only a weak oceanic constraint, mostly from the oceanic

transport when other ocean areas (middle–low latitudes, for instance) are strongly constrained by ocean observations. For the NAG, due to its wind-driven nature, a full atmospheric (wind and temperature) constraint mostly determines its seasonal–interannual variability (Fig. 4b), and a coherent combination of atmospheric and oceanic constraints is able to produce a quite high monitoring skill (Fig. 7).

b. AMOC

As a consequence of reproducing the key components of the North Atlantic climate system, all 5 examined observing systems are able to reproduce the variability of the AMOC to some degree, evidenced by the high ACCs (>.8) (column 11 of Table 2) and the overall truth-like variations of the time series of the estimated AMOC indices (Fig. 5). However, the accuracy of the reconstructed AMOC mean state and the time scale of the best-estimated variability are different for each observing system.

Comparing the time series of the AMOC produced by ocean-only observing systems O_{XBT} (dashed green) and O_{Argo} (dashed red) to their counterpart with the addition of atmospheric observations (solid green and solid red), referred to the time series produced by O_{SSTt}^{Atm} (blue), we found that the sea surface forcings provided by the atmosphere and SST observations contribute mainly to the interannual variability of the AMOC. While the subsurface temperature observations provided by O_{XBT} tend to constrain the decadal-scale tendency of the AMOC, the addition of the salinity and deep-ocean observations in O_{Argo} improves the intradecadal variability and refines the decadal regime transition greatly (Fig. 5). However, although forced by the generated SSTs from the oceanic constraint, the internally free atmosphere in the assimilations of O_{XBT} and O_{Argo} cannot provide a significantly corrected NAO signal owing to strong atmospheric internal variability. This explains the incorrect interannual variability of the AMOC estimated by O_{XBT} and O_{Argo}. Thus, a coherent combination of the atmosphere and ocean observations within a coupled system is necessary to reconstruct the variability of the AMOC accurately. As shown in Fig. 5 and columns 10 and 11 of Table 2, only when the atmospheric wind and temperature data are incorporated into the coupled system do both the XBT and Argo observations (O_{XBT}^{Atm} and O_{Argo}^{Atm}) resolve the phase of the AMOC variation very well and produce a much higher ACC with the truth. In particular, as a coupled product of the reconstructed NAO, LSW, GSW, and NAG as shown in Fig. 4, while the twenty-first-century climate observing system reconstructs the AMOC by 90%, without direct salinity and deep ocean observations the twentieth-century climate observing system only reconstructs the AMOC

by 52%, both including a small uncertainty (0.5% sdv) (columns 4 and 5 of Fig. 7).

Given the importance of the heat/salt transport carried by the AMOC to global climate (e.g., Latif et al. 2004; Zhang et al. 2006), here we analyze the vertical structure of the AMOC mean state constrained by various observing systems. Although Figs. 5 and 6 show that the capability of an observing system to reconstruct the AMOC mean state and variability is basically consistent, some points about the accuracy of the estimated AMOC mean state are still worthy of being addressed. First, compared to the constraint of an ocean observing system (O_{XBT} or O_{Argo}), the constraint of surface forcings (O_{SSTt}^{Atm}) produces a more consistent AMOC mean state (Fig. 6b), although the accuracy of the estimated decadal variability and regime transition is lower. Second, Figs. 6c and 6d clearly show that, consistent with the variability estimate for the AMOC, the time-mean transport constrained by O_{Argo} is much better than the one constrained by O_{XBT}. A question could be asked whether it is the Argo's direct salinity observation, the Argo's temperature observation at depth, or their combination that is responsible for the improvement of the O_{Argo} estimate for the North Atlantic climate system. The fact that the XBT coverage in the upper ocean is much denser than the Argo, especially in the western boundary area (see Figs. 3a,b), indicates that increasing the temperature coverage for upper ocean observations does not help, even in the crucial area for estimating the AMOC. A reasonable speculation is that the Argo's direct salinity observation may play a critical role because it improves the density structure so as to improve the estimate of buoyancy. However, a clear-cut mechanism requires further research work to clarify, including an experiment in which only Argo temperatures are assimilated. This shall be further investigated in follow-up studies. Third, while the addition of the surface forcing constraint to O_{XBT} increases the AMOC error over the middle–upper ocean but reduces the error at the bottom ocean (Fig. 6e), the combination of the atmospheric and Argo constraints consistently reduces the AMOC error dramatically, except for the subtropical bottom ocean (Fig. 6f). The too strong southward transport at the subtropical bottom ocean in O_{Argo}^{Atm} suggests an imbalance between the direct ocean data adjustment from the Argo observations and the ocean's response to the surface forcing constraint. The reason for the too strong southward transport also shall be further investigated in follow-up studies to improve the physical balance and vertical coherence of ECDA's data adjustments.

Analyzing the variability of the NAG, LSW, and GSW indices and comparing it to that of the AMOC in different time scales may provide a preliminary understanding for the contributions of NAG, LSW, and GSW to the AMOC

variability. Comparing the time series of LSW produced by 2 model simulations and 5 assimilations in Fig. 4d to the corresponding AMOC time series in Fig. 5, we found that LSW generally exhibits the low-frequency (decadal) variability as in the AMOC. A bandpass analysis shows that, while the 1–2-yr fluctuations in the AMOC are correlated well with the variability of NAG, only a weak correlation was found between the 5–6-yr AMOC fluctuations and the GSW variability (see also Figs. 4b,c and 5). These results suggest that, while the NAG impacts the interannual variability of the AMOC, GSW may only have some weak impact on the subdecadal variability. Interestingly, when both the atmospheric and subsurface oceanic observations are used, the GSW monitoring skill increases significantly compared to the case that uses either atmospheric or oceanic observations alone (Fig. 7)—for example, the GSW monitoring skill of $O_{\mathrm{Argo}}^{\mathrm{Atm}}$ increasing by 78% from 35% of O_{Argo}. This may be related to sea ice activities that freely respond to the atmospheric and oceanic observational constraints in the present ECDA. The GSW index here represents the water property of the intermediate and deep layer of the Fram Strait, which links sea ice export from the Arctic to the North Atlantic (Hu et al. 2009; Hopkins 1991). The variability of sea ice is determined by both the atmospheric (dynamic) and oceanic (thermodynamic) conditions. In an assimilation over a few decades, the surface forcings only ($O_{\mathrm{SSTt}}^{\mathrm{Atm}}$) cannot constrain the variability of GSW skillfully (Figs. 4c and 7), suggesting that reconstructing GSW requires both the atmospheric and subsurface oceanic constraints to work together more coherently. In contrast to GSW, again, the NAG as a wind-driven oceanic circulation system can be recovered to some degree by every observing system, either atmospheric, oceanic, or a combination (Figs. 4b and 7). In particular, it is recovered up to 83% with 0.5% sdv by $O_{\mathrm{Argo}}^{\mathrm{Atm}}$, which combines the atmospheric and oceanic constraints very well. These results explain that each of the examined observing systems has its own capability to recover the AMOC variability in some time scales as well as the time-mean state to some degree as shown in Figs. 5 and 6.

5. Summary and discussions

We assess the adequacy of various routine observing networks for monitoring the Atlantic meridional overturning circulation and related North Atlantic climate quantities. Our approach is to use the synthetic "observations" (Sobs) derived by sampling from the GFDL CM2.0 climate model according to the spatial and temporal coverage of various observing systems. It is shown that the twentieth-century XBT and twenty-first-century Argo networks, when combined with atmospheric temperature

and winds through a coupled data assimilation system, are able to recover the phase of the temporal variation of the AMOC—as indicated by a 0.98 linear correlation between the AMOC derived from the Sobs and the truth AMOC. However, while the $O_{\mathrm{Argo}}^{\mathrm{Atm}}$ Sobs successfully reconstructs 90% of the AMOC as a whole measurement of the monitoring by normalized root-mean-squared error, the $O_{\mathrm{XBT}}^{\mathrm{Atm}}$ network reconstructs only 52%, suggesting an important role of salinity and deeper-ocean observations present in the Argo network.

An important goal of this work is to develop a system for AMOC monitoring and prediction. An accompanying study (S. Zhang et al. 2010, unpublished manuscript) will further show that, using these observing networks combined with a coupled assimilation system, a decadal-scale predictability of the AMOC within the context of a perfect model framework does exist.

Considerable work remains before models can be used in conjunction with modern observing systems to estimate and predict the AMOC. As one important example, the current work does not take model bias into account. Some research work has started to address the bias issue between a model and the real-world observations, for example, assimilating anomalies rather than the full values into the model (Smith et al. 2007). As an alternative approach to address the model bias issue, a multimodel ensemble assimilation system is under development at GFDL, and it may be useful to relax the negative impact of individual model bias on assimilation results. In such a system, the error statistics used to extract observational information are based on a multimodel ensemble, and the generated analysis can be accordingly distributed into different model spaces. It is expected that such a multimodel ensemble assimilation system not only improves the estimate of anomalies but also controls the climatological drift to some degree. In addition, further studies should also include specialized observations such as the Rapid Climate Change (RAPID) mooring array (Kanzow et al. 2007; Cunningham et al. 2007) into the monitoring system to obtain more insights on the impact of the observing system on the monitoring and prediction of the North Atlantic climate system.

REFERENCES

Anderson, J. L., 2003: A local least squares framework for ensemble filtering. *Mon. Wea. Rev.,* **131,** 634–642.

Balmaseda, M. A., D. Dee, A. Vidard, and D. T. Anderson, 2007a: A multivariate treatment of bias for sequential data assimilation: Application to the tropical oceans. *Quart. J. Roy. Meteor. Soc.,* **133,** 167–179.

——, G. C. Smith, K. Haines, D. Anderson, T. N. Palmer, and A. Vidard, 2007b: Historical reconstruction of the Atlantic meridional overturning circulation from the ECMWF operational ocean reanalysis. *Geophys. Res. Lett.,* **34,** L23615, doi:10.1029/2007GL031645.

Bryden, H. L., H. R. Longworth, and S. A. Cunningham, 2005: Slowing of the Atlantic meridional overturning circulation at 25°N. *Nature,* **438,** 655–657.

Cunningham, S. A., and Coauthors, 2007: Temporal variability of the Atlantic meridional overturning circulation at 26.5°N. *Science,* **317,** 935–938.

Dee, J., 2005: Bias and data assimilation. *Quart. J. Roy. Meteor. Soc.,* **131,** 3323–3343.

——, and A. M. Sliva, 1998: Data assimilation in the presence of forecast bias. *Quart. J. Roy. Meteor. Soc.,* **124,** 269–295.

Delworth, T. L., 1996: North Atlantic interannual variability in a coupled ocean–atmosphere model. *J. Climate,* **9,** 2356–2375.

——, and R. J. Greatbatch, 2000: Multidecadal thermohaline circulation variability driven by atmospheric surface flux forcing. *J. Climate,* **13,** 1481–1495.

——, and M. E. Mann, 2000: Observed and simulated multidecadal variability in the Northern Hemisphere. *Climate Dyn.,* **16,** 661–676.

——, S. Manabe, and R. J. Stouffer, 1993: Interdecadal variations of the thermohaline circulation in a coupled ocean–atmosphere model. *J. Climate,* **6,** 1993–2011.

——, and Coauthors, 2006: GFDL CM2 global coupled climate models. Part I: Formulation and simulation characteristics. *J. Climate,* **19,** 643–674.

Eden, C., and T. Jung, 2001: North Atlantic interdecadal variability: Oceanic response to the North Atlantic oscillation (1865–1997). *J. Climate,* **14,** 676–691.

Enfield, D. B., A. M. Mestas-Nuñez, and P. J. Trimble, 2001: The Atlantic Multidecadal Oscillation and its relation to rainfall and river flows in the continental U.S. *Geophys. Res. Lett.,* **28,** 2077–2080.

Folland, C. K., T. N. Palmer, and D. E. Parker, 1986: Sahel rainfall and worldwide sea temperatures, 1901–85. *Nature,* **320,** 602–607.

GFDL Global Atmospheric Model Development Team, 2004: The new GFDL global atmosphere and land model AM2–LM2: Evaluation with prescribed SST simulations. *J. Climate,* **17,** 4641–4673.

Gnanadesikan, A., and Coauthors, 2006: GFDL's CM2 global coupled climate models. Part II: The baseline ocean simulation. *J. Climate,* **19,** 675–697.

Goldenberg, S. B., C. W. Landsea, A. M. Mestas-Nuñez, and W. M. Gray, 2001: The recent increase in Atlantic hurricane activity: Causes and implications. *Science,* **293,** 474–479.

Griffies, S. M., 2005: Some ocean model fundamentals. *Ocean Weather Forecasting: An Integrated View of Oceanography,* E. P. Chassignet and J. Verron, Eds., Springer, 19–74.

——, and K. Bryan, 1997: Predictability of North Atlantic multidecadal climate variability. *Science,* **275,** 181–184.

——, and Coauthors, 2005: Formulation of an ocean model for global climate simulations. *Ocean Sci.,* **1,** 45–79.

Häkkinen, S., and P. B. Rhines, 2004: Decline of subpolar North Atlantic circulation during the 1990s. *Science,* **304,** 555–559.

Hátún, H., A. B. Sandø, H. Drange, B. Hansen, and H. Valdimarsson, 2005: Influence of the Atlantic Subpolar Gyre on the thermohaline circulation. *Science,* **309,** 1841–1844.

Hilmer, M., and T. Jung, 2000: Evidence for recent change in the link between the North Atlantic Oscillation and Arctic sea ice export. *Geophys. Res. Lett.,* **27,** L010944, doi:10.1029/1999GL010944.

Hopkins, T., 1991: The GIN Sea—A synthesis of its physical oceanography and literature review 1972–1985. *Earth Sci. Rev.,* **30,** 175–318.

Hu, A., G. A. Meehl, W. Han, and J. Yin, 2009: Transient response of the MOC and climate to potential melting of the Greenland Ice Sheet in the 21st century. *Geophys. Res. Lett.,* **36,** L10707, doi:10.1029/2009GL037998.

Hunke, E. C., and J. K. Dukowicz, 1997: An elastic–viscous–plastic model for sea ice dynamics. *J. Phys. Oceanogr.,* **27,** 1849–1867.

Ivchenko, V. O., N. C. Wells, and D. L. Aleynik, 2006: Anomaly of heat content in the northern Atlantic in the last 7 years: Is the ocean warming or cooling? *Geophys. Res. Lett.,* **33,** L22606, doi:10.1029/2006GL027691.

Jazwinski, A. H., 1970: *Stochastic Processes and Filtering Theory.* Academic Press, 376 pp.

Johnson, H. L., D. P. Marshall, and D. A. Sproson, 2007: Reconciling theories of a mechanically driven meridional overturning circulation with thermohaline forcing and multiple equilibria. *Climate Dyn.,* **29,** 821–836.

Jungclaus, J. H., H. Haak, M. Latif, and U. Mikolajewicz, 2005: Arctic North Atlantic interactions and multidecadal variability of the meridional overturning circulation. *J. Climate,* **18,** 4013–4031.

Kalnay, E., 2003: *Atmospheric Modeling, Data Assimilation, and Predictability.* Cambridge University Press, 341 pp.

——, and Coauthors, 1996: The NCEP/NCAR 40-Year Reanalysis Project. *Bull. Amer. Meteor. Soc.,* **77,** 437–471.

Kanzow, T., and Coauthors, 2007: Observed flow compensation associated with the MOC at 26.5°N in the Atlantic. *Science,* **317,** 938–941.

Latif, M., and Coauthors, 2004: Reconstructing, monitoring, and predicting multidecadal-scale changes in the North Atlantic thermohaline circulation with sea surface temperature. *J. Climate,* **17,** 1605–1614.

Levitus, S., J. I. Antonov, and T. P. Boyer, 2005: Warming of the World Ocean. *Science,* **287,** 2225–2229.

Lock, A. P., A. R. Brown, M. R. Bush, G. M. Martin, and R. N. B. Smith, 2000: A new boundary layer mixing scheme. Part I: Scheme description and single-column model tests. *Mon. Wea. Rev.,* **128,** 3187–3199.

Moorthi, S., and M. J. Suarez, 1992: Relaxed Arakawa-Schubert: A parameterization of moist convection for general circulation models. *Mon. Wea. Rev.,* **120,** 978–1002.

Randall, D. A., and Coauthors, 2007: *Climate models and their evaluation. Climate Change 2007: The Physical Science Basis,* S. Solomon et al., Eds., Cambridge University Press, 589–662.

Smith, D. M., S. Cusack, A. W. Colman, C. K. Folland, G. R. Harris, and J. M. Murphy, 2007: Improved surface temperature prediction for the coming decade from a global climate model. *Science,* **317,** 796–799.

Stouffer, R. J., A. J. Weaver, and M. Eby, 2004: A method for obtaining pre-twentieth century initial conditions for use in climate change studies. *Climate Dyn.,* **23,** 327–339.

Sutton, R. T., and D. L. R. Hodson, 2005: Atlantic Ocean forcing of North American and European summer climate. *Science,* **309,** 115–118.

Thompson, D. W. J., and J. M. Wallace, 2000: Annular modes in the extratropical circulation. Part I: Month-to-month variability. *J. Climate,* **13,** 1000–1016.

Winton, M., 2000: A reformulated three-layer sea ice model. *J. Atmos. Oceanic Technol.,* **17,** 525–531.

Wunsch, C., and P. Heimbach, 2006: Estimated decadal changes in the North Atlantic meridional circulation and heat flux 1993–2004. *J. Phys. Oceanogr.,* **36,** 2012–2024.

Wyman, B. L., 1996: A step-mountain coordinate general circulation model: Description and validation of medium-range forecasts. *Mon. Wea. Rev.,* **124,** 102–121.

Zhang, R., T. L. Delworth, and I. M. Held, 2006: Can the Atlantic Ocean drive the observed multidecadal variability in Northern Hemisphere mean temperature? *Geophys. Res. Lett.,* **34,** L02709, doi:10.1029/2006GL028683.

Zhang, S., and J. L. Anderson, 2003: Impact of spatially and temporally varying estimates of error covariance on assimilation in a simple atmospheric model. *Tellus,* **55A,** 126–147.

——, M. J. Harrison, A. Rosati, and A. Wittenberg, 2007: System design and evaluation of coupled ensemble data assimilation for global oceanic climate studies. *Mon. Wea. Rev.,* **135,** 3541–3564.

——, A. Rosati, and M. J. Harrison, 2009: Detection of multidecadal oceanic variability by ocean data assimilation in the context of a ''perfect'' coupled GCM. *J. Geophys. Res.,* **114,** C12018, doi:10.1029/2008JC005261.